AIP | The Journal of Chemical Physics

The electronic spectrum of NOCl: Photofragment spectroscopy, vector correlations, and ab initio calculations

Y. Y. Bai, A. Ogai, C. X. W. Qian, L. Iwata, G. A. Segal, and H. Reisler

Citation: The Journal of Chemical Physics **90**, 3903 (1989); doi: 10.1063/1.455801
View online: http://dx.doi.org/10.1063/1.455801
View Table of Contents: http://scitation.aip.org/content/aip/journal/jcp/90/8?ver=pdfcov
Published by the AIP Publishing

The electronic spectrum of NOCl: Photofragment spectroscopy, vector correlations, and *ab initio* calculations[a]

Y. Y. Bai, A. Ogai,[b] C. X. W. Qian, L. Iwata,[b] G. A. Segal, and H. Reisler
Department of Chemistry, University of Southern California, Los Angeles, California 90089-0482

(Received 31 October 1988; accepted 13 December 1988)

The electronic absorption spectrum of NOCl in the region 620–180 nm is assigned by using vector properties of the NO photofragment and the results of *ab initio* calculations at the CI level. In assigning the electronic spectrum, we take into account the recoil anisotropy, rotational alignment, and Λ-doublet populations of NO, as well as the calculated vertical excitation energies, oscillator strengths, and the nature of the orbitals involved in the transitions. In the experiments, we use expansion-cooled samples and measure the recoil anisotropy parameters from the Doppler profiles of selected NO $\mathrm{A}\,^2\Sigma^+ \leftarrow \mathrm{X}\,^2\Pi$ rotational lines. The alignment parameters and Λ-doublet populations are derived from the rotational spectra using different laser polarizations and excitation–detection geometries. The theoretical calculations treat all low-lying singlet and triplet states. The calculations yield least energy paths for the excited states, with optimized r_{NO} and ClNO angle as a function of r_{ClN}, as well as the angular dependences of the potentials and oscillator strengths of the singlet–singlet transitions. The following assignments are proposed for the main absorption bands: (1) **E** band—$T_1(1\,^3A'')\leftarrow S_0(1\,^1A')$; the transition borrows intensity by mixing with remote singlet states, predominantly the $4\,^1A'$ state; (2) **D** and **C** bands—$S_1(1\,^1A'')\leftarrow S_0(1\,^1A')$; the **C** band corresponds to excitation of v_1' in S_1; (3) **B** band—$S_3(2\,^1A')\leftarrow S_0(1\,^1A')$; (4) **A** band—$S_5(4\,^1A')\rightarrow S_0(1\,^1A')$. The assignments proposed here are in full agreement with all the experimental observations and the results of the calculations. Despite the shallow minima calculated for the T_1 and S_1 surfaces, dissociation on all the surfaces is fast, and the implications of the results to the dissociation dynamics are discussed.

I. INTRODUCTION

Assigning the electronic spectra of molecules with dissociative states is often hindered by lack of structure (e.g., rotational and vibrational peaks that serve as fingerprints). Spectral overlap of lifetime broadened transitions further complicates the assignments, since weak electronic transitions may be completely hidden under strong, broad features. Correct assignments of the excited states are important in photodissociation studies where a description of the photodissociation dynamics in terms of detailed motions on a specific potential energy surface (PES) is required. Fortunately, today there exist a variety of polarized laser spectroscopic techniques[1–6] that, in conjunction with tunable laser photolysis, photofragment yield (PHOFRY) spectroscopy and expansion cooling of the parent molecules, can facilitate the assignments of the absorption spectra of dissociative states. Measurements of vector properties and correlations yield information on the symmetry of the transitions, the direction of the transition dipole moment μ relative to the molecular frame, and the orientation of the participating orbitals.[1–6] The experimental results can be interpreted with the aid of accurate *ab initio* calculations to yield fairly unique assignments of the electronic transitions.

The important vectors that play a role in the elucidation of the electronic structure of dissociative states are μ (which is preferentially aligned along the polarization vector $\mathbf{E}_{\mathrm{ph}}$ of the photolysis laser), the recoil velocity of the photofragment $\mathbf{v}$, its rotational angular momentum $\mathbf{J}$, and the direction of the singly occupied π lobes of radicals in Π electronic states. For triatomic molecules, the situation is further simplified by the sensible assumptions that the dissociation is planar, the recoil is nearly axial and the diatomic fragment rotates in the plane of the parent molecule.[1] In this case, since $\mathbf{J}$ is perpendicular to the plane of the parent and $\mathbf{v}$ is in the plane, we get trivially that $\mathbf{J}$ is perpendicular to $\mathbf{v}$. The pairwise correlations that can be obtained by using polarized lasers for photolysis and detection of the photofragments are[1,5] (i) the direction of μ relative to $\mathbf{v}$[1,3,5]; (ii) the direction of μ relative to $\mathbf{J}$, and therefore the plane of the parent molecule[1,4,5]; and (iii) the direction of the singly occupied π lobe relative to $\mathbf{J}$, which in the absence of extensive electronic reorganization during dissociation can be related to the initially excited orbital in the parent molecule.[6] This property is independent of nuclear motion prior to dissociation, since it is given in the molecular frame.

NOCl is an excellent prototypical molecule for application of the vector correlation methods, since it possesses several low lying dissociative excited states that give rise to electronic transitions in the UV and visible. Its 300 K spectrum was obtained in 1939 by Goodeve and Katz[7] and shows several partially overlapping broad peaks labeled A to K in the original publication in order of increasing wavelength (Fig.

---

[a] Research supported by the National Science Foundation, and the Army Research Office under the auspices of the Center for the Study of Fast Transient Processes.

[b] NSF Predoctoral Fellow.

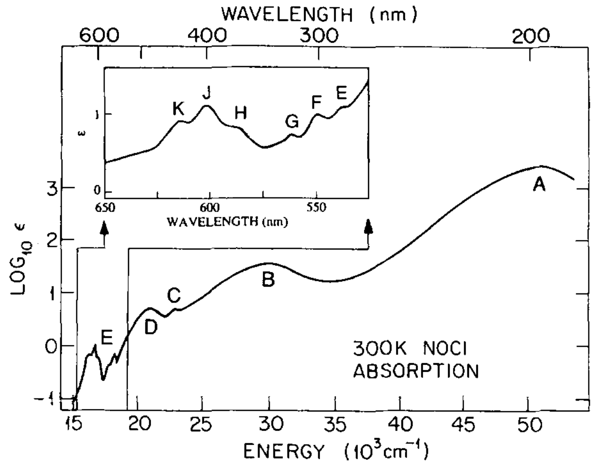

FIG. 1. The absorption spectrum of 300 K NOCl as measured by Goodeve and Katz (Ref. 7). The lowest absorption band, called the E band, corresponds to a series to diffuse bands (see inset) assigned E–K in Ref. 7.

1). Although the spectrum was not assigned, Goodeve and Katz were able, by inspection, to reach the following conclusions[7]: (i) The lowest absorption peaks E to K arise from transitions to vibrational levels of a single dissociative electronic state (hereafter labeled the **E** band). This transition, which is very weak, may be spin forbidden. (ii) The stronger **A**, **B**, and **D** bands are associated with repulsive states. (iii) The **C** band is separated from the **D** band by 1670 cm^{-1}, an interval which is close to the frequency of the NO vibration in NOCl, and thus may be part of the **D** band.

In 1983, Solgadi *et al.* published the first *ab initio* CI calculations on NOCl and obtained vertical excitation energies for the singlet states.[8] They proposed that the observed absorption bands be assigned to the lowest three singlet $^1A''$ and $^1A'$ states.[8] Busch and Wilson studied the photofragment spectroscopy of NOCl at 347 nm and showed that the **B** band is of A' symmetry with μ nearly parallel to **v**.[9] Very recently, Bruno *et al.* reported a one-laser pump-and-probe study of the photodissociation of 300 K NOCl in the region of the **D** and **C** bands and obtained the symmetry of the transitions from the measured Doppler profiles of NO rotational lines.[10] Based on their observations[10] and *ab initio* calculations,[8] they proposed that the **E**, **D**, **C**, and **B** bands arise from excitation to $S_1(1\ ^1A'')$, $S_2(2\ ^1A'')$, $S_3(2\ ^1A')$, and $S_4(3\ ^1A')$, respectively.[10]

In an independent study of the photodissociation of jet-cooled NOCl, we reached a similar conclusion regarding the **D** band, but the assignment of the **B** band to the $3\ ^1A' \leftarrow 1\ ^1A'$ transition presented a difficulty.[11] According to *ab initio* calculations,[8] this transition predominantly involves $a' \leftarrow a'$ electronic excitation that should have resulted in a preferential population of the in-plane singly occupied NO π^* orbital $[\Pi(A')$ Λ-doublet component$]$,[6(c)] whereas the experimental results show a large preference for the out-of-plane $\Pi(A'')$ component.[11] In an effort to find the source of this discrepancy, we extended the measurements to other band systems, and also carried out new *ab initio* calculations on the low-lying states of NOCl. The calculations reported here are more complete than the previous ones in that we include triplet states since the spin–orbit splitting in Cl is substantial (880 cm^{-1}). We also carry out more complete explorations of the potential energy surfaces, and report oscillator strengths for the singlet transitions. Based on the new calculations and the experimental results, we reassign the electronic spectrum, and in particular we propose that the lowest absorption band (the **E** band) arises from a singlet–triplet transition, $T_1(1\ ^3A'') \leftarrow S_0(1\ ^1A')$, which borrows intensity from a strong remote $^1A'$ transition. The new assignments are in full agreement with all the experimental observations reported to date.

The paper is organized as follows. In Sec. II we give a brief description of the experimental arrangement, and in Sec. III we present the experimental results and their analyses. Section IV describes the computational methods and results. In Sec. V we discuss the electronic structure of NOCl and the new proposed assignments. In closing, we comment on the implications of our findings to the photodissociation dynamics of NOCl.

II. EXPERIMENTAL

The experimental arrangement was very similar to the one used previously,[11,12] and only details specific to the present experiment are described. The fluorescence chamber was of octagonal shape, and can accommodate several laser excitation–detection geometries. Premixed NOCl samples (10/500 Torr in He) were prepared and expanded via a pulsed valve (Lasertechnics, 500 μm diam. orifice, $\sim$200 μs pulse duration) into the fluorescence chamber. The photolysis laser was a Nd:YAG laser pumped dye laser system (Quanta Ray DCR1A/PDL1), and the probe laser radiation was obtained from an excimer laser pumped dye laser system (Lambda Physik EMG 101 MSC/FL 2001). The output at 450 nm was frequency doubled with a BBO crystal (CSK Ltd.), and the NO fragments were probed by one-photon LIF via the $A\ ^2\Sigma^+ \leftarrow X\ ^2\Pi$ transition at $\sim$226 nm. The fluorescence was detected with a solar blind PMT (Hamamatsu R166UH) through an interference filter (Corion, 300 nm, 85 nm bandwidth). The intensity of the probe laser beam was maintained at $< 40\ \mu J$ in order to avoid saturation, and dissociation of NOCl by the 226 nm radiation in particular. Although the 300 K absorption cross section of NOCl at 226 nm is much larger than at the photolysis wavelengths used in these experiments, dissociation and detection by the probe laser involve sequential absorption of two photons, and this process is largely eliminated when $I_{pr} \ll I_{ph}$.[11]

Two configurations of the laser and detector were used. In most of the sub-Doppler resolution spectroscopy experiments, the two laser beams and the pulsed nozzle were mutually orthogonal, and the PMT was located at 45° in the same plane as the laser beams. An intracavity etalon (FSR = 1 cm^{-1}) was used to narrow the laser linewidth, and the frequency was pressure tuned with N_2. The combined laser bandwidth and velocity spread of NO in the nozzle expansion were determined from the Doppler profiles of premixed He/NO samples,[12] and the measured linewidth was < 0.15 cm^{-1}.

In the spatial anisotropy and Λ-doublet experiments, the two laser beams were collinear and counterpropagating, but perpendicular both to the PMT and to the pulsed valve.

The polarization of the photolysis laser was rotated with a half-wave plate, and the desired polarization component was further selected with a Rochon polarizer. The probe laser was maintained at a vertical polarization. The timing sequence was controlled by a homemade digital delay generator with 20 ns increments, and the delay between the pump and probe lasers was typically < 80 ns. The observed LIF signals were normalized to both laser intensities. Usually, the signals from 30 to 100 laser firings were averaged for each data point.

NOCl (Matheson) was purified by trap-to-trap distillations. Due to the existence of equilibrium between NOCl and NO, it was impossible to completely eliminate NO contamination. However, the expansion-cooled NO contamination gives rise predominantly to $J'' < 5.5$, and the distributions reported here were corrected by carrying out on/off experiments. When expanding NOCl in He, clustering became a problem at high He and NOCl concentrations. Apparently, dissociation of the clusters results in less NO recoil anisotropy than dissociation of the monomers. We find that with $P_{He} < 500$ Torr and $< 2\%$ NOCl, the results are independent of the expansion conditions, and these pressures and concentration ratios were maintained throughout the experiments.

III. EXPERIMENTAL RESULTS AND ANALYSES

Since NOCl belongs to the C_s symmetry group, only two types of transitions, A' (μ in the molecular plane) and A'' (μ perpendicular to the molecular plane), are defined. The μ–$\mathbf{v}$ correlation is obtained from the sub-Doppler profiles and yields the recoil anisotropy parameter β.[3] The limiting values of β are 2 and -1 for $\mu \| \mathbf{v}$ and $\mu \perp \mathbf{v}$, respectively. For NOCl, since $\mathbf{v}$ is in the molecular plane, $\beta = 2$ corresponds to an A' transition, but $\beta = -1$ can correspond to either A' or A'' transitions, and in order to distinguish between these two cases, the μ–$\mathbf{J}$ correlation is required as well.[4,5] The transition is of A' symmetry when $\mu \perp \mathbf{v}$ and $\mu \perp \mathbf{J}$, whereas it is of A'' symmetry when $\mu \perp \mathbf{v}$ and $\mu \| \mathbf{J}$, assuming $\mathbf{v} \perp \mathbf{J}$. The μ–$\mathbf{J}$ correlation is obtained from the rotational alignment parameter $A_0^{(2)}$ whose limiting values are 0.8 and -0.4 for $\mu \| \mathbf{J}$ and $\mu \perp \mathbf{J}$, respectively.[4,5] A β value between the limiting ones corresponds, in the case of fast dissociation, either to an A' transition where the μ–$\mathbf{v}$ angle is at an intermediate value between 0° and 90°, or to a case where both A'' and A' transitions are reached simultaneously at a particular photodissociation wavelength. In the latter case, tuning the photolysis laser wavelength usually yields β values which vary smoothly with excitation energy.

For NO fragments, another useful correlation is the orientation of the singly occupied π^* lobe relative to $\mathbf{J}$.[6] This orientation can be obtained from the Λ-doublet populations; for the $A\,^2\Sigma^+ \leftarrow X\,^2\Pi$ transition, Q lines and P/R lines probe Λ-doublet components that are perpendicular to—and in—the plane of NO rotation, respectively.[6] Those have recently been denoted $\Pi(A'')$ and $\Pi(A')$, respectively.[6(c)] In the absence of significant charge rearrangement during the dissociation, a preference for the $\Pi(A'')$ or $\Pi(A')$ Λ-doublet component indicates that the singly occupied orbital in the excited state of NOCl is of a'' or a' symmetry, respectively.

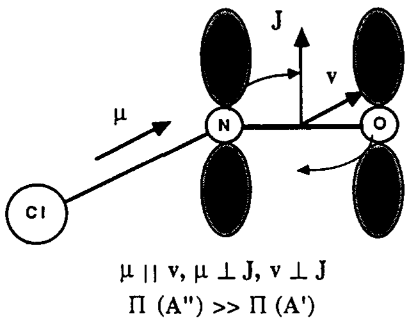

FIG. 2. A schematic representation of the μ–$\mathbf{v}$–$\mathbf{J}$ and Λ-doublet correlations. In this specific example, which describes **B** band excitation, $\mu \| \mathbf{v}$, $\mu \perp \mathbf{J}$, $\mathbf{v} \perp \mathbf{J}$, and $\Pi(A'') \gg \Pi(A')$.

This information can then be compared with the results of *ab initio* calculations in order to assign the transition. An illustrative example of the relevant vector correlations is depicted in Fig. 2 for excitation in the **B** band.

A detailed description of the methodologies used in analyzing the results is given in our previous publication.[11] We follow established procedures, and use the approach developed by Dixon.[5] Below, we describe our findings concerning the **E**, **D**, **C**, and **B** bands. The results of the measurements of the vector properties are also summarized in Table I.

A. NO recoil anisotropies

The correlation between μ and $\mathbf{v}$ can be obtained from the Doppler profiles of selected rotational lines of NO. The Doppler line shape is given by[3,5]

$$g(\chi_D) = [1 + \beta P_2(\cos\alpha) P_2(\chi_D)](2\Delta\nu_0)^{-1}, \qquad (1)$$

where χ_D is the Doppler shift which is equal to $(\mathbf{v}\cdot\mathbf{k}/c)\nu_0$, $g(\chi_D)$ is the line-shape function, P_2 is the second order Legendre polynomial, α is the angle between $\mathbf{E}_{ph}$ and $\mathbf{k}_{pr}$, $\Delta\nu_0$ is the maximum frequency shift from line center, and β is the recoil anisotropy parameter. Obviously, the Doppler line shapes depend strongly on the excitation–detection geometry, as well as on the symmetry of the transition. Doppler profiles for selected rotational lines of NO were obtained with two laser polarization configurations: $\mathbf{E}_{ph} \perp \mathbf{k}_{pr}$ (vertical polarization) and $\mathbf{E}_{ph} \| \mathbf{k}_{pr}$ (horizontal polarization). In Fig. 3 we present typical Doppler profiles of several NO rotational lines obtained following excitation in the **E**, **D**, and **B**

TABLE I. Vector and scalar properties of NO($X\,^2\Pi$).

Band	Transition Symmetry	β	A_0^2	NO v'' state	Preferred Λ doublet
E[a]	A'	$\mathbf{v} \| \mu$	$\mathbf{J} \perp \mu$	0	$\Pi(A'')$
E[b]	A'	$\mathbf{v} \| \mu$	$\mathbf{J} \perp \mu$	1	$\Pi(A'')$
D	A''	$\mathbf{v} \perp \mu$	$\mathbf{J} \| \mu$	0	$\Pi(A'')$
C	A''	$\mathbf{v} \perp \mu$	$\mathbf{J} \| \mu$	1	$\Pi(A'')$
B	A'	$\mathbf{v} \| \mu$	$\mathbf{J} \perp \mu$	0	$\Pi(A'')$

[a] NO($v'' = 0$) is produced with excitation in the H, J, and K bands (see Fig. 1).

[b] NO($v'' = 1$) is produced with excitation in the E, F, and G bands.

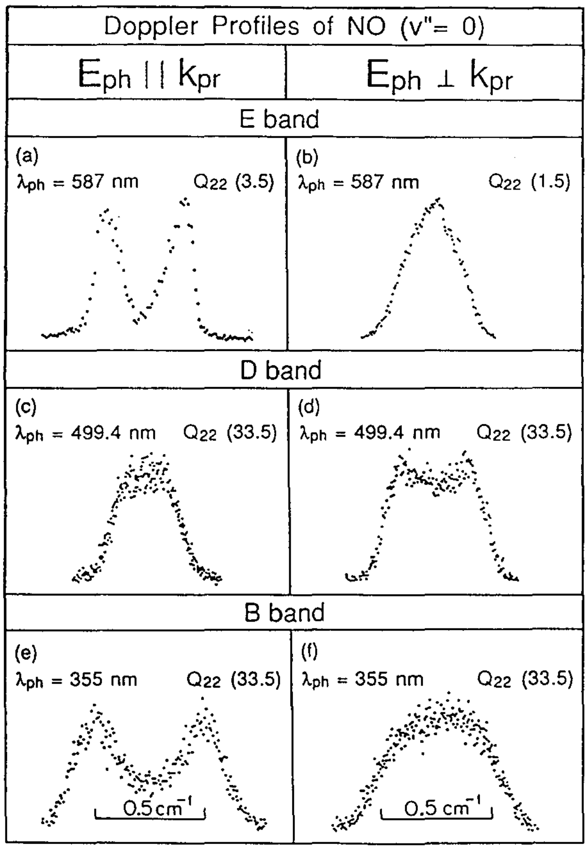

FIG. 3. Doppler profiles of NO($X\,^2\Pi_{3/2}$, $v''=0$) Q_{22} lines. The left- and right-hand-side entries are associated with $\mathbf{E}_{ph}$ parallel and perpendicular, respectively, to $\mathbf{k}_{pr}$. The lasers configuration in all the panels except (b) is $\mathbf{k}_{pr}\perp\mathbf{k}_{ph}$. In panel (b) $\mathbf{k}_{pr}\|\mathbf{k}_{ph}$ was employed. This affects the Doppler profiles only through the **v**–**J** correlation, and has only a small effect on the line shape.

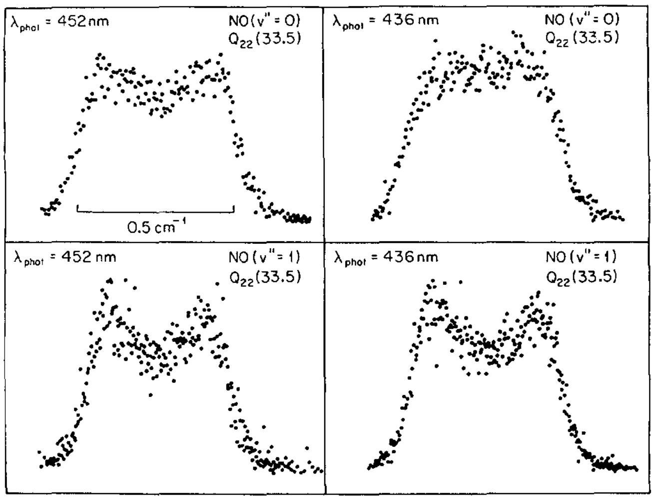

FIG. 4. Doppler profiles of NO($^2\Pi_{3/2}$) $Q_{22}(33.5)$ in the region of the C band. The laser excitation–detection geometry is $\mathbf{k}_{pr}\|\mathbf{k}_{ph}$ and $\mathbf{E}_{pr}\|\mathbf{E}_{ph}$. The lower panels show two NO($v''=1$) profiles which are typical of a perpendicular transition. NO($v''=0$) profiles exhibit an increasing parallel component with decreasing wavelength, and two typical profiles are shown in the upper panels.

bands. From the shapes of the profiles and their variation with the photolysis laser polarization,[3,5] it is evident that excitations in the **E** and **B** bands derive from parallel transitions, while a perpendicular transition is responsible for the **D** band. All the profiles shown in Fig. 3 were simulated by convoluting the calculated line shapes with the combined laser bandwidth and NO velocity spread (see Sec. II), using a 13 000 cm^{-1} bond dissociation energy. With **E**, **D**, and **B** band excitations, we obtain $\beta = 1.9 \pm 0.1$, -1.0 ± 0.1, and 1.8 ± 0.2 respectively, and the results are independent of the probed $\mathbf{J}''$ and the excitation wavelength within each band. It should be pointed out, however, that the above analysis does not include the effects of the **v**–**J** correlation. For NOCl, **v** is perpendicular to **J**, but the effects of the correlation are not large and are included in the error bars. *Q* and *P*, *R* branch lines give slightly different values of β, but the distinction between parallel and perpendicular transitions is obvious. With **E** band excitation, mostly low NO rotational levels are populated, and the profiles are the least affected by the **v**–**J** correlation, since alignment effects are small.[4,5]

With **C** band excitation, the Doppler profiles are particularly intriguing. When monitoring NO($v''=0$), the Doppler profiles obtained following 430–460 nm photolysis are typical of a mixed parallel-perpendicular transition, as reported previously by Bruno *et al.* for 450 nm photolysis.[10] We find that the parallel transition component increases with the decrease in photodissociation wavelength. In contrast, only a perpendicular transition is required to simulate the Doppler profiles obtained when monitoring NO($v''=1$) at the same wavelength region. Typical Doppler profiles at 452 and 436 nm are shown in Fig. 4 for the $Q_{22}(33.5)$ lines of NO($v''=0$) and NO($v''=1$). Similar Doppler profiles are obtained when monitoring other rotational levels or branches, and for both spin–orbit states of NO. Evidently, at these wavelengths NO($v''=1$) profiles have a much larger perpendicular component than the Doppler profiles associated with NO($v''=0$). At the peak of the **C** band (i.e., 436 nm), the NO($v''=1$) Doppler profiles can be fit by a purely perpendicular transition, while those of NO($v''=0$) have a substantial parallel character. We point out that a quantitative estimate of the ratio of parallel to perpendicular transitions must take into account the dependences of the fluorescence intensities and the β parameters on the excitation–detection geometries. The relative fluorescence intensities resulting from parallel and perpendicular transitions depend on the monitored NO rotational branch, and the specific polarizations and the propagation directions of both lasers, and must be treated explicitly when deriving the branching ratios.

In order to assign the **C** band, we also obtained the PHOFRY spectra in the **C** band region by monitoring NO($v''=0$) and NO($v''=1$). In Fig. 5, we present PHOFRY spectra obtained when monitoring $Q_{22}(33.5)$ for both vibrational levels and the differences between the two spectra are apparent. When monitoring NO($v''=1$), the peak in the PHOFRY spectrum coincides with the 300 K **C** absorption peak (i.e., ~440 nm). This peak is completely missing when monitoring NO($v''=0$), and the spectra can be described as a smooth transition from the **D** to the **B** band. A similar behavior is observed when monitoring other rotational lines and branches, and we propose (see Sec. V) that

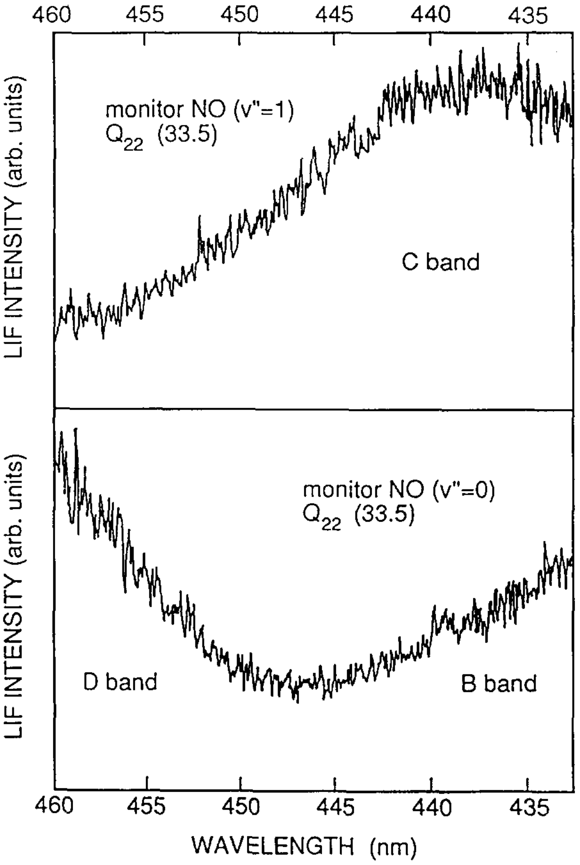

FIG. 5. PHOFRY spectra in the region of the **C** band. The upper panel is obtained by monitoring NO($v''=1$) and shows a peak corresponding to the **C** band in the absorption spectrum. This peak is absent when monitoring NO($v''=0$) (lower panel), and the PHOFRY spectrum in this region is best described as a smooth transition from the **D** to the **B** band.

the **C** band arises from NO stretch excitation in NOCl via the same perpendicular transition that gives rise to the **D** band. This excitation results predominantly in production of NO($v''=1$).

B. Rotational alignment and Λ-doublet ratios

In fast photofragmentation processes,the rotational distributions cannot be inferred trivially from the raw experimental line intensities due to alignment of the fragments. Consequently, the relative line intensities depend on the particular lasers–detector–polarization configuration. As in our previous work,[11] we follow the treatment of Dixon,[5] and describe the rotational line intensities by

$$I_{ie}=AS_{ie}N_i\,[b_0+b_1\beta_0^2(02)], \tag{2}$$

where A is a constant, I_{ie} is the intensity of a line originating from ground state level i to excited state e, S_{ie} is the rotational line strength, N_i is the population of level i, b_0 and b_1 are constants which are a function of J_i'', the rotational branch and the specific lasers–detector configuration, and $\beta_0^2(02)$ is the bipolar moment describing rotational alignment.[5] $\beta_0^2(02)$ is related to the more commonly used rotational alignment parameter $A_0^{(2)}$ by[4]

$$A_0^{(2)}=0.8\beta_0^2(02). \tag{3}$$

In our analyses, we compare two spectra obtained with the lasers–detector configurations described in Sec. II, one where $\mathbf{E}_{\rm ph}\parallel\mathbf{E}_{\rm pr}$ and a second where $\mathbf{E}_{\rm ph}\perp\mathbf{E}_{\rm pr}$ (referred to as geometries I and II, respectively, in Ref. 5), and we also take account of the spectral overlap between branches. A least-squares fit program was used to normalize the two spectra using separate $\beta_0^2(02)$ constants for the $^2\Pi_{1/2}$ and $^2\Pi_{3/2}$ states. With **D** band excitation, we found previously, in agreement with Ref. 10, that $A_0^{(2)}=0.64\pm0.10$ for both NO spin–orbit states, indicating that the transition is of A'' symmetry.[11] We also showed that the $v''=0$ rotational populations are inverted, peaking at $J''\cong30.5$ with bell-shaped distributions, and in addition, the $^2\Pi_{3/2}$ state is more populated than the lower $^2\Pi_{1/2}$ state. Similar results were obtained by Huber and co-workers for NO($v''=1$) following 470 nm excitation.[10]

The NO($v''=0$) rotational distributions (uncorrected for alignment effects) obtained with excitation in the **B** band are shown in Fig. 6 for the two different laser polarization

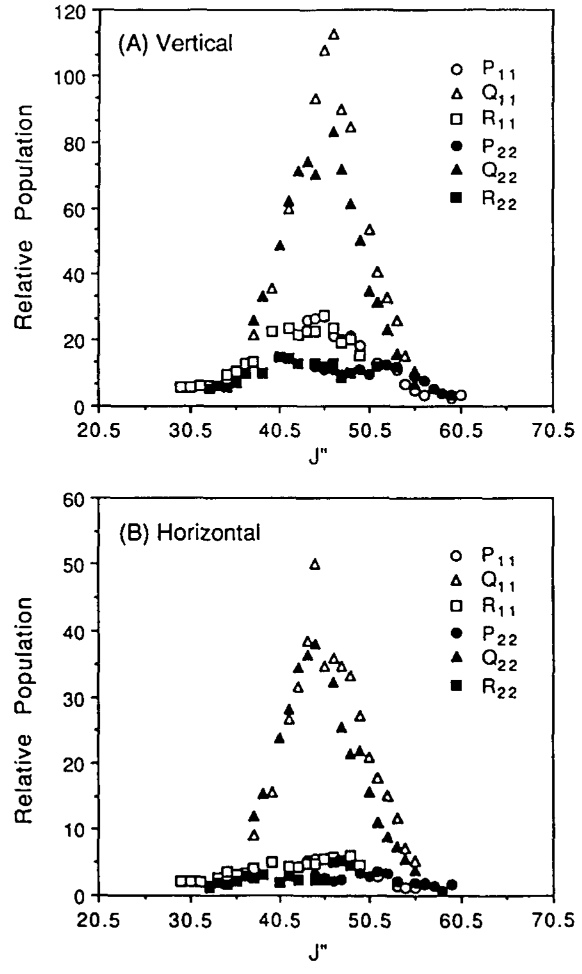

FIG. 6. NO($v''=0$) rotational level distributions following **B** band excitation at 355 nm. The distributions are obtained from the LIF spectra by dividing the rotational line intensities by the corresponding line strengths. Results obtained with vertical ($\mathbf{E}_{\rm pr}\parallel\mathbf{E}_{\rm ph}$) and horizontal ($\mathbf{E}_{\rm pr}\perp\mathbf{E}_{\rm ph}$) photolysis laser polarizations are shown in panels (A) and (B), respectively. In both panels $\mathbf{k}_{\rm pr}$ is parallel to $\mathbf{k}_{\rm ph}$ and $\mathbf{E}_{\rm pr}$ is vertically polarized. Notice that the *P,R* lines are more intense in the vertical polarization lasers configuration, indicating that $\mathbf{J}\perp\mu$ is preferred.

configurations described above. As with **D** band excitation, the distributions are bell shaped and peak at high J''. However, the $^2\Pi_{1/2}$ spin state is slightly more populated than the $^2\Pi_{3/2}$ state. Inspection of the two spectra reveals that the intensity of Q lines relative to P, R lines is larger in panel A than in B, indicating that the $\mu \perp \mathbf{J}$ orientation is preferred. A quantitative estimate of the rotational alignment is not as accurate as for the **D** band because of the very low intensity of the P and R branch lines (see below). However, an analysis similar to the one reported for the **D** band yields $A_0^{(2)} = -0.32 \pm 0.1$, and this result confirms that the **B** transition is of A' symmetry.

Representative NO($^2\Pi_{3/2}$, $v'' = 0$) rotational distributions obtained with **E** band excitation are shown in Fig. 7. [The population of NO($^2\Pi_{1/2}$) in this case is very small.] With 587 nm excitation, a multimodal distribution is obtained with a large component at low J''. The P_{12} and Q_{22} lines of the NO($^2\Pi_{3/2}$) state both correspond to the $\Pi(A'')$ Λ-doublet component, and their relative intensities should be equal in the absence of alignment.[13] However, as is clearly evident in Fig. 7, P_{12} lines are more intense than Q_{22} lines with the vertical polarization configuration. This indicates that $\mu \perp \mathbf{J}$ is preferred, in accord with the assignment of A' symmetry for the transition. The rotational distributions within the **E** band depend strongly on the absorption peak that is excited by the photolysis laser, indicating state specific photodissociation dynamics.[14] Nonetheless, all derive from typical A' transitions with **v** nearly parallel to μ.

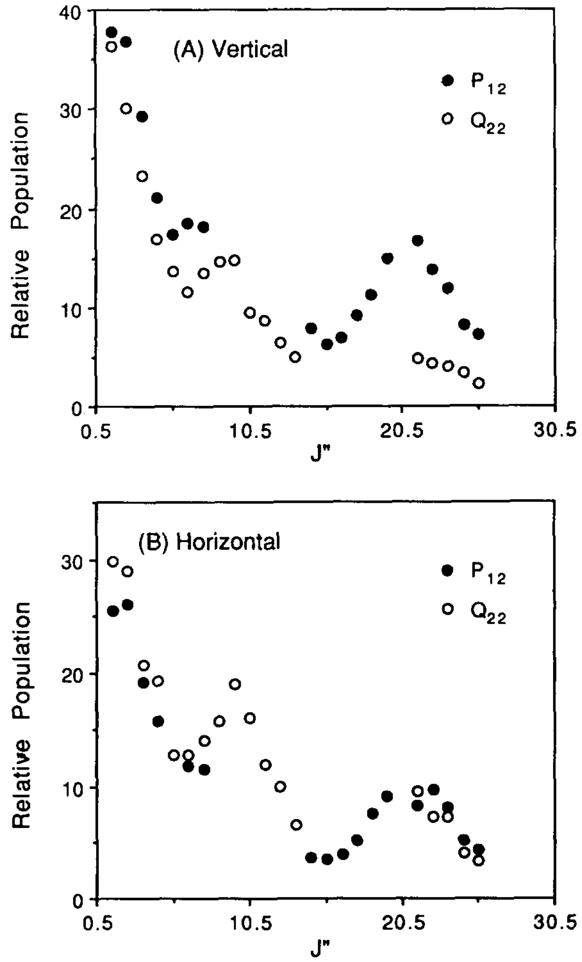

FIG. 7. NO($v'' = 0$) rotational level distributions following **E** band excitation at 587 nm. The distributions are obtained from the LIF spectra by dividing the line intensities by the corresponding line strengths. The laser configurations are the same as in Fig. 6. Notice that although both P_{12} and Q_{22} branch lines derive from the same Λ-doublet component, $\Pi(A'')$, the relative intensities of the P_{12} lines are higher in panel (A) than in (B). This is due to rotational alignment and indicates that $\mu \perp \mathbf{J}$ is favored (see the text).

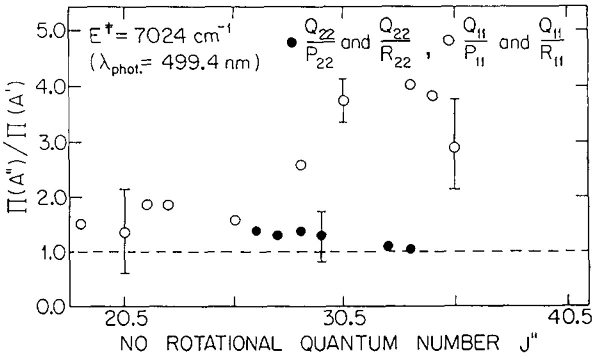

FIG. 8. NO Λ-doublet population ratios in the $^2\Pi_{1/2}$ (○) and $^2\Pi_{3/2}$ (●) states of NO($v'' = 0$) obtained following **D** band excitation. $\Pi(A'')$ and $\Pi(A')$ refer to the singly occupied $p\pi$ NO orbital perpendicular to and in the plane of rotation of NO, respectively.

By comparing the populations derived from Q and R or P lines, the relative populations of the two Λ-doublet components can be obtained. The results as a function of J'' are summarized in Figs. 8 and 9 for excitation in the **D** and **B** bands, respectively. We include only lines that are not severely overlapped and whose intensities are relatively large. The plotted populations are corrected for the effect of rotational alignment. The $\Pi(A'')$ Λ-doublet component is preferred with excitation in both bands. The maximum $\Pi(A'')/\Pi(A')$ ratio is greater with **B** band excitation [$\Pi(A'')/\Pi(A') \sim 10$ for the highest J'']; however, the degree of alignment of the π lobes increases with J'', and for similar J'' the Λ-doublet ratio is similar in the two bands. A notable exception is the lack of Λ-doublet preference in NO($^2\Pi_{1/2}$) produced via excitation in the **D** band, as discussed in a previous publication.[11] With **E** band excitation, mainly low NO J'' states, which are not expected to exhibit a Λ-doublet prefer-

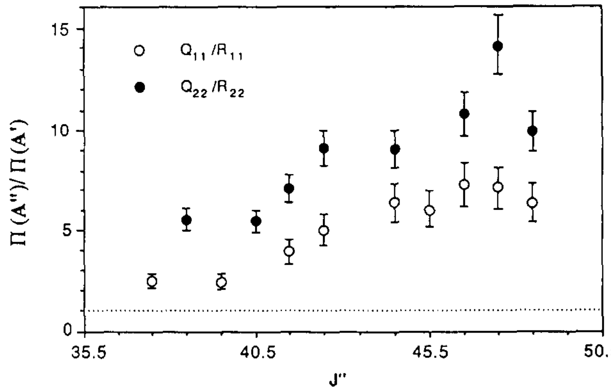

FIG. 9. NO Λ-doublet population ratios in the $^2\Pi_{1/2}$ (○) and $^2\Pi_{3/2}$ (●) states of NO($v'' = 0$) obtained following **B** band excitation.

ence, are produced. However, the highest J'' states obtained with 587 nm excitation exhibit preferential population of the $\Pi(A'')$ component. Thus, excitations of NOCl in the **E**, **D**, and **B** bands all lead to preferential population of the NO π^* orbital perpendicular to the plane of rotation of NO, and hence the NOCl molecular plane. The results of the vector properties are summarized in Table I.

TABLE II. Molecular orbtials involved in the lowest excited states of NOCl.

Symmetry	MO	Eignevalue (a.u.)	Description
a'	18	0.0704	$\mathrm{Cl}p_x + \mathrm{NO}\pi_z^*$
a''	17	0.0409	$\mathrm{NO}\pi_z^*$
a'	16	−0.4245	$\mathrm{Cl}p_x + \mathrm{O}p_x$
a'	15	−0.4516	$\mathrm{Cl}p_y$
a''	14	−0.4520	Clp_z
a''	13	−0.7323	$\mathrm{NO}\pi_z$

IV. COMPUTATIONAL METHODS AND RESULTS

All the calculations reported here were carried out using Dunning's[15] double zeta quality $(9s5p/4s2p)$ contracted atomic orbital basis set augmented by a set of six d polarization functions on each atom with Gaussian exponents of 0.60 for chlorine, 0.80 for nitrogen, and 0.85 for oxygen. Hartree–Fock calculations performed using the GAUSSIAN 82 system of programs[16] were followed by large scale configuration interaction (CI) calculations involving all single and double hole–particle excitations from a multiconfiguration set of reference configurations. The $n = 1$ and 2 electrons of chlorine were frozen as were the $n = 1$ electrons of nitrogen and oxygen. The reference configurations were chosen on the basis of their importance to the electronic state under study, and the resulting CI problem was solved using the program PEPCI.[17] As a general rule, all configurations which had a coefficient in the final wave function greater than 0.1 were included in the reference space. All geometries were optimized by finite difference using a quadratic fitting function.

The basis set which we have employed is compact, and we have previously found it to be quite efficient in representing the lower electronic excited states of polyatomic molecules.[18] In this paper, our primary focus is upon low-lying states of NOCl that lie in the region of the **B** absorption band and below (i.e., less than ~4 eV above the ground state), so we have not chosen to augment the basis set with radially expanded (Rydberg) functions. While our basis set is adequate for this purpose, we must expect that its flexibility is limited at higher energies. For this reason, our calculations in the region of the **A** band, which lies more than 6 eV above the ground state, are more approximate than those at lower energies. They are, however, qualitatively correct, and, as noted by Solgadi *et al.*,[8] the first true Rydberg transition is expected to lie at approximately 7.50 eV, well above the region under study here.

The experimental equilibrium geometry of NOCl is $r_{\mathrm{NO}} = 1.13$ Å, $r_{\mathrm{ClN}} = 1.975$ Å, and $<\mathrm{ClNO} = 113.3°$,[19] and 16 molecular orbitals are occupied in the ground state of NOCl. In our coordinate system, the y axis is along the NO bond, and Cl lies in the xy plane. At infinite separation, NO possesses doubly degenerate π and π^* molecular orbitals that may be viewed as lying in the x and z directions. Of these, the x component resolves to a' in NOCl while z passes to an a'' orbital. At this geometry and in this basis set, the molecular orbitals which are principally involved in the excited states are summarized in Table II, and a pictorial view is given in Fig. 10. The highest occupied molecular orbitals 14–16 are predominantly the three Cl p orbitals which are degenerate in the atom and nearly degenerate in NOCl. Excitations from these to MO 17, which is predominantly of NO π_z^* character, would be expected to lie close to each other in energy and this accounts for the richness of the spectrum below 4 eV. In addition, MO 18 lies but 0.8 eV above the LUMO, and single hole particle excitations to this MO also lead to fairly low-lying electronic states.

The calculated vertical excitation energies and the electric dipole oscillator strengths are summarized in Table III. As shown by the principal single hole particle excitations involved, the nature of these states is consistent with the qualitative considerations described above. Table IV, which shows the gross electronic charge density on each atom for each state as calculated from the final CI vector using the Mulliken approximation, summarizes the nature of these transitions in another way. Here we see that the lowest excited states involve some degree of charge transfer from Cl to NO.

The dynamics of the photofragmentations of NOCl to $\mathrm{Cl}(^2P_{1/2,3/2})$ and $\mathrm{NO}(^2\Pi_{1/2,3/2})$ depends upon the nature of the three-dimensional PES upon which dissociation takes place. We have therefore calculated least energy paths for a number of electronic states, optimizing r_{NO} and the ClNO angle as a function of r_{ClN}. The numerical results of these calculations are given in Table V, and the minimized potential energy curves are shown in Fig. 11. The results shown in Table V differ importantly from those presented by Solgadi *et al.*,[8] who optimized the ClNO bond angle as a function of r_{ClN} but fixed r_{NO} at 1.13 Å, in that the lowest singlet excited state $1\,^1A''$ has a potential energy minimum rather than being simply repulsive. The minimum lies at 1.68 eV, whereas

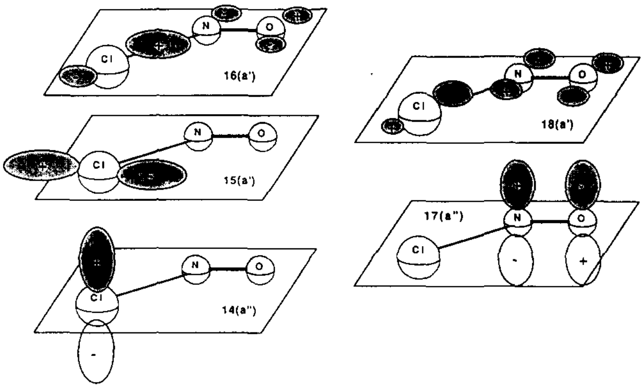

FIG. 10. A pictorial view of the relevant occupied and unoccupied orbitals involved in the electronic transitions. A fuller description of each orbital is given also in Table II. We note that in MO 16 most of the calculated electron distribution is around Cl and O, with very little around N.

TABLE III. Vertical excitation energies and oscillator strengths.[a]

State	Primary excitation	E_{calc} (eV)	E_{exp} (eV)[b]	f_{calc}	f_{exp}[c]	Band
$S_0(1\,^1A')$		0.0		0.0		
$T_1(1\,^3A'')$	$17a'' \leftarrow 16a'$	1.75	2.06	0.0	1×10^{-5}	**E**
$S_1(1\,^1A'')$	$17a'' \leftarrow 16a'$	2.32	2.64	2×10^{-4}	9×10^{-5}	**D, C**
$T_2(1\,^3A')$	$18a' \leftarrow 16a'$	2.90		0.0		
$T_3(2\,^3A')$	$17a'' \leftarrow 14a''$	3.13		0.0		
$T_4(2\,^3A'')$	$17a'' \leftarrow 15a'$	3.29		0.0		
$S_2(2\,^1A'')$	$17a'' \leftarrow 15a'$	3.37		8×10^{-6}		
$S_3(2\,^1A')$	$17a'' \leftarrow 14a''$	3.70	3.72	1×10^{-1}	1×10^{-3}	**B**
$T_5(3\,^3A')$	$18a' \leftarrow 15a'$	4.48		0.0		
$S_4(3\,^1A')$	$18a' \leftarrow 15a'$	4.79		1×10^{-3}		
$S_5(4\,^1A')$	$18a' \leftarrow 16a'$	7.18	6.30	1.0	0.5	**A**

[a] Energies relative to $1\,^1A'$ $E_{\text{eq}} = -589.153\,392$ a.u. at the experimental equilibrium geometry: $r_{\text{NCL}} = 1.975$ Å, $r_{\text{NO}} = 1.13$ Å, $<\text{ClNO} = 113.3°$.

[b] E_{exp} is defined as the peak of the absorption band.

[c] The experimental oscillator strengths were calculated from the spectra and extinction coefficients given in Refs. 7 and 20.

the calculated vertical excitation energy is 2.32 eV and the experimental dissociation energy is 1.6 eV.[9] A similar, and considerably deeper well is also found for the analogous triplet state, where $E_{\text{min}} = 1.16$ eV and the vertical excitation energy is at 1.75 eV (Tables III and V).

The source of the difference, of course, is a moderately strong coupling between the r_{NO} and ClNO bending coordinates. As shown in Table V, the optimum value for r_{NO} separation at $r_{\text{ClN}} = 1.975$ Å (i.e., the ground state equilibrium separation in NOCl) is in the vicinity of 1.21 Å for all the excited electronic states which we consider. The coupling between r_{NO} and ClNO bending can be seen from the variation of energy for these states as a function of ClNO angle and r_{ClN} at $r_{\text{NO}} = 1.13$ Å, the ground state separation, and $r_{\text{NO}} = 1.21$ Å. This comparison, which is basically two particular sheets cut from the full three-dimensional surfaces, is shown in Table VI and Fig. 12.

As seen in Table III, we differ from all previous authors in assigning the lowest energy absorption system, which we term **E**, to a spin-forbidden transition to the $1\,^3A''$ state. This is discussed in Sec. V, along with the assignments of the other transitions.

V. DISCUSSION

A. Assignment of the electronic spectrum

In assigning the electronic spectrum, we take into account the directional properties of the NO fragment (e.g., recoil anisotropy, rotational alignment, Λ-doublet populations), as well as the calculated vertical excitation energies, oscillator strengths, and the nature of the orbitals involved in the transitions. The assignments proposed here are in agreement with all the experimental observations, but differ from previous assignments in two important ways. First, we include the singlet–triplet transitions, and second, we neglect excitations to singlet states whose oscillator strengths are small compared with those of adjacent transitions. The proposed assignments are summarized in Table III, and the important molecular orbitals are depicted in Fig. 10. In discussing the proposed assignments, we start with singlet–singlet transitions, since our reasons for assigning the lowest absorption band to the spin-forbidden $1\,^3A'' \leftarrow 1\,^1A'$ transition thus become clearer.

We assign the $S_1(1\,^1A'')$ state to the **D** absorption band. The computed excitation energy is 2.32 eV, which compares favorably with the experimental band maximum at 2.64 eV. The calculated oscillator strength, 2×10^{-4}, is considerably larger than the estimated experimental value, 9×10^{-5}, since the calculations assume a Franck–Condon factor of 1.00 and thus give only upper limits. The calculated equilibrium NO bond for this state at the moment of excitation (i.e., when r_{ClN} is 1.975 Å) is 1.21 Å, while that of the ground state is 1.15 Å. We therefore expect a considerable reduction in the total, as distinguished from the electronic oscillator strength due to a rather poor Franck–Condon factor for this transition. As previously noted, all the excited states have an elongated NO bond length relative to the ground state, so we expect that all the calculated oscillator strengths will be

TABLE IV. Atomic charges in some states of NOCl.

State	$1\,^1A'$	$1\,^3A''$	$1\,^1A''$	$1\,^3A'$	$2\,^3A''$	$2\,^3A'$	$2\,^1A''$	$2\,^1A'$	$3\,^3A'$	$3\,^1A'$	$4\,^1A'$
Cl	−0.170	+0.556	−0.041	−0.041	+0.496	+0.430	+0.962	+0.850	+0.227	+0.092	−0.188
N	+0.143	−0.310	+0.061	−0.045	−0.265	−0.292	−0.585	−0.563	−0.159	−0.069	+0.084
O	+0.027	−0.246	−0.020	+0.086	−0.231	−0.138	−0.377	−0.287	−0.068	−0.023	+0.104

TABLE V. Geometrically optimized potential energy surfaces of NOCl for some electronic states which lead to NO($X\,^2\Pi$) + Cl(^2P).

State	$r_{\rm NCl}$ (Å)	$r_{\rm NO}$ (Å)	ClNO (deg)	Energy (eV)$^{\rm a}$
$1\,^1A'$	1.975	1.15	115	0.00
	2.075	1.15	114	0.08
	2.175	1.16	114	0.21
	2.400	1.16	112	0.61
$1\,^3A''$	1.975	1.21	120	1.60
	2.075	1.17	120	1.18
	2.175	1.16	118	1.16
	2.400	1.16	114	1.35
$1\,^1A''$	1.975	1.19	120	2.27
	2.075	1.17	120	1.69
	2.175	1.16	120	1.62
	2.400	1.16	120	1.64
$1\,^3A'$	1.975	1.21	166	2.22
	2.075	1.17	158	1.92
	2.175	1.16	156	1.71
	2.400	1.16	154	1.33
$2\,^1A''$	1.975	1.21	108	3.26
	2.075	1.17	118	2.65
	2.175	1.16	120	2.38
	2.400	1.16	120	2.07
$2\,^1A'$	1.975	1.21	112	3.56
	2.075	1.17	112	2.88
	2.175	1.16	112	2.53
	2.400	1.16	112	2.19

$^{\rm a}$Energies relative to $1\,^1A'$ $E_{\rm eq} = -589.154\,168$ a.u. at the calculated geometry: $r_{\rm NCl} = 1.975$ Å, $r_{\rm NO} = 1.15$ Å, $<$ClNO = 115°.

large compared to the experimental values. The Doppler profiles indicate that at all wavelengths within the D band, μ is perpendicular to **v** with $\beta \sim -1$, and from the alignment data we conclude that the transition is of A'' symmetry. In spite of the fact that the optimized potential curve along the reaction coordinate exhibits a shallow minimum, the dissociation is fast, as is manifest in the large recoil anisotropy and rotational alignment parameters. The experimental Λ-doublet data for NO($^2\Pi_{1/2}$),which yield $\Pi(A'') > \Pi(A')$, are consistent with this assignment, since excitation is predominantly to MO 17 whose symmetry is a'' (Fig. 10), as is the overall symmetry of the transition. The intriguing difference between the Λ-doublet preference for NO($^2\Pi_{1/2}$) and NO($^2\Pi_{3/2}$)[11] requires a deeper scrutiny. As shown in Fig. 11, the $S_1(1\,^1A'')$ state is crossed by the $T_2(1\,^3A')$ state whose vertical excitation energy is 2.90 eV and whose equilibrium geometry is close to linear (Table VI). No vibration exists which can couple states of A' and A'' symmetry, but they can be coupled by spin within the C_s point group, and this coupling occurs in an M_s specific fashion. If such coupling is efficient, it could account for the state-specific Λ-doublet behavior.

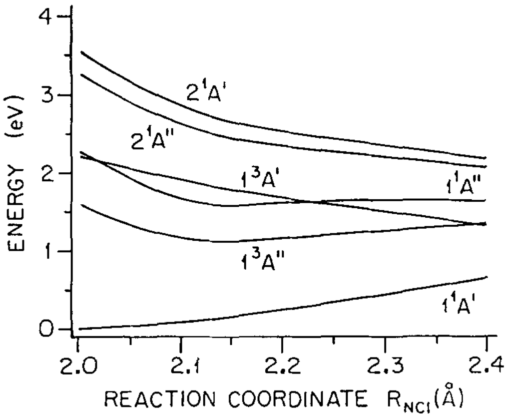

FIG. 11. Optimized least energy paths along the reaction coordinate $r_{\rm ClN}$ obtained by optimizing $r_{\rm NO}$ and the ClNO angle. Notice the shallow minima in the $1\,^3A''$ and $1\,^1A''$ curves.

TABLE VI. Angular potential energy variation of ClNO.

ClNO (deg)	Energy (eV)$^{\rm a}$ $1\,^1A'$	$1\,^3A''$	$1\,^1A''$	$1\,^3A'$	$2\,^1A''$	$2\,^1A'$
	$r_{\rm NO} = 1.13$ Å		$r_{\rm NCl} = 1.975$ Å			
111.3	0.023	1.815	2.347	3.165	3.361	3.644
115.3	0.019	1.747	2.340	2.985	3.418	3.680
119.3	0.086	1.752	2.351	2.938	3.503	3.722
125.3	0.211	1.785	2.352	2.850	3.689	3.843
129.3	0.334	1.806	2.375	2.795	3.807	3.926
139.3	0.773	1.885	2.396	2.655	3.995	4.116
162.3	2.409	2.168	2.940	2.224	5.004	4.556
	$r_{\rm NO} = 1.21$ Å		$r_{\rm NCl} = 1.975$ Å			
112.3	0.120	1.638	2.336	2.965	3.286	3.600
116.3	0.129	1.612	2.319	2.905	3.306	3.618
120.3	0.199	1.600	2.318	2.864	3.392	3.674
124.3	0.280	1.608	2.325	2.814	3.509	3.764
128.3	0.407	1.630	2.365	2.741	3.633	3.839
154.3	1.830	2.028	2.811	2.299	5.492	4.399
162.3				2.232		

$^{\rm a}$Energy relative to $1\,^1A'$ $E_{\rm eq} = -589.154\,168$ a.u., at the calculated equilibrium geometry: $r_{\rm NCl} = 1.975$ Å, $r_{\rm NO} = 1.15$ Å, $<$ClNO = 115°.

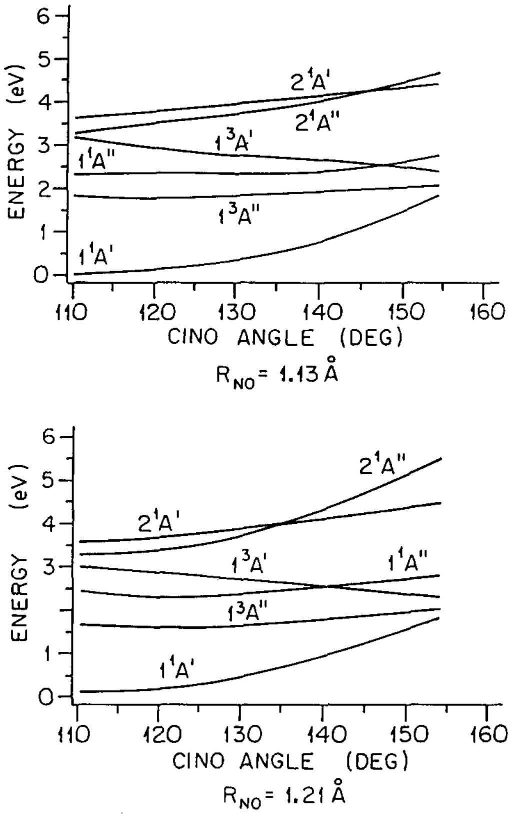

FIG. 12. The angular dependence of the potential surfaces at $r_{\mathrm{ClN}} = 1.975$ Å, and $r_{\mathrm{NO}} = 1.13$ Å (upper panel) and 1.21 Å (lower panel). The r_{NO} values correspond to vertical excitation and optimized NO internuclear separation in the upper surface, respectively.

The next excited singlet state, $S_2(2\ {}^1A'')$, is calculated to have a very small electronic dipole oscillator strength, 8.6×10^{-6}, a value which should be further diminished by a poor Franck–Condon factor. Thus, it is probably hidden under the strong **B** band.

The nature of the **B** band is, however, consistent with the computed features of the $S_3(2\ {}^1A')$ state. The calculated excitation energy is 3.70 eV which compares favorably with the absorption maximum at 3.72 eV. The computed oscillator strength is again much larger than the observed value, undoubtedly due to a poor Franck–Condon factor. The experimental recoil anisotropy parameter is typical of a parallel transition with μ nearly parallel to **v**, confirming the A' overall nature of the upper state, and the rotational alignment is consistent with this interpretation. This is in agreement with the calculations which yield a 17.3° angle between the direction of μ and the N–Cl. Finally, the Λ-doublet data show $\Pi(A'') \gg \Pi(A')$, an observation consistent with the fact that this state results from excitation to MO 17 whose symmetry is a''. This orbital is predominantly of NO π_z^* character (Table II), suggesting that very little charge redistribution takes place during the dissociation, despite the final state interactions that result in large rotational excitation in the NO fragment.

The broad **A** band is probably composed of a number of excited states, but one of them is undoubtedly the $S_5(4\ {}^1A')$ state which has a large oscillator strength. This state is calculated to lie at 7.18 eV, a value which compares poorly with the observed absorption maximum at 6.30 eV. However, as discussed earlier, we ascribe this error to the limitations inherent in our Gaussian basis set; we are not able to well describe excitations at such high energy since they generally involve expansion of the average electronic distribution to larger distances from the nuclear frame. The calculated angle between μ and N–Cl bond is 8.9°, which is characteristic of a parallel transition.

The assignments which we have just described seem to fit all available data well with the exceptions that we have found no singlet states which may be reasonably assigned to the **E** and **C** bands. With excitation in the **E** band, both the recoil anisotropy and the rotational alignment are typical of a parallel transition, implying that μ must lie in the molecular plane, and is nearly parallel to **v**. The oscillator strength, however, is quite small, and Goodeve and Katz suggest that it may involve a forbidden transition.[7] We ascribe this transition to spin–orbit (**L·S**) coupling between the $1\ {}^3A''$ state, which is calculated to lie at 1.75 eV, and higher lying strongly absorbing singlet states of A' symmetry. As shown in Table III, the experimental oscillator strength is $\sim 1\times 10^{-5}$. To estimate the intensity borrowing by mixing with a remote perturber, we calculate the first order mixing coefficient between the $1\ {}^3A''$ state and a singlet state of A' symmetry:[21]

$$C_{1\,{}^3A'',{}^1A'} = \langle 1\ {}^3A'' | H_{\mathrm{so}} | {}^1A' \rangle / \Delta E,$$

where ΔE is the energy difference between the two states. The oscillator strength is given by $|C|^2 \times f_{{}^1A'}$, where $f_{{}^1A'}$ is the oscillator strength of the singlet–singlet transition from which intensity is borrowed. Assuming that the upper limit for the H_{so} matrix element is given by the Cl spin–orbit parameter ($\sim 500\ \mathrm{cm}^{-1}$),[21] we can calculate upper limits for the oscillator strengths derived from intensity borrowing by mixing with higher ${}^1A'$ states whose oscillator strengths are known. For mixing with $S_3(2\ {}^1A')$, we find, using the calculated value for the vertical excitation energy and the experimental oscillator strength, that

$$f_{1\,{}^3A''} \cong [(500\ \mathrm{cm}^{-1}/12\,985\ \mathrm{cm}^{-1})^2 \times 10^{-3}] \cong 1.5\times 10^{-6}.$$

A similar computation of the mixing coefficient with $S_5(4\ {}^1A')$ yields.

$$f_{1\,{}^3A''} \cong [(500\ \mathrm{cm}^{-1}/33\,469\ \mathrm{cm}^{-1})^2 \times 0.5] \cong 1\times 10^{-4}.$$

In this calculation the experimental values for the excitation energy and the oscillator strength (see Table III) are used. These values compare favorably with the experimental oscillator strength for the **E** band, and thus spin–orbit coupling can account for the intensity and symmetry of the transition. We emphasize that although mixing with singlet states is responsible for the oscillator strength and thus determines the values of the β and $A_0^{(2)}$ parameters, only 2% of the $4\ {}^1A'$ wave function is required to yield the experimentally observed oscillator strength. Thus, the T_1 state has predominantly $1\ {}^3A''$ character, and the Λ-doublet populations reflect the a'' symmetry of the excited state orbital (MO 17).

The partially overlapping absorption peaks designated E–K in Ref. 7 all belong to the **E** band. As suggested by Goodeve and Katz, the peaks separated by 380 cm^{-1} can be assigned to excitation of bending vibrations in $T_1(^3A'')$, whereas the groups of peaks H, J, K, which are separated from the E, F, G group by 1580 cm^{-1}, arises from excitation of one quantum of NO stretch in T_1 (the band origin is assumed to be at 16 240 cm^{-1}).[7] It is noteworthy that photolysis at wavelengths corresponding to these latter peaks yields predominantly NO($v''=1$), whereas NO($v''=0$) is mainly produced following excitation in the E, F, G wavelength region.[14]

We believe that excitation to $S_1(1\,^1A'')$ is responsible for both the **D** and the **C** bands, as the two peaks are separated by ~ 1670 cm^{-1},[7] a value which is close to the NO stretch frequency (i.e., the **C** band arises from excitation of S_1 with one quantum of NO stretch). This assignment is based on the following observations: (i) In the PHOFRY spectrum, a peak similar to the **C** band appears only when monitoring NO($v''=1$) (Fig. 5). (ii) The NO($v''=1$) recoil anisotropy parameter corresponds to a predominantly perpendicular transition (Fig. 4). (iii) At comparable wavelengths, rotational lines in NO($v''=0$) show a large parallel component indicating a large contribution from dissociation on the $S_3(2\,^1A')$ surface (Fig. 4). (iv) The PHOFRY spectra obtained when monitoring Q_{22}, R_{22}, and Q_{11} lines of $v''=0$ do not show a peak corresponding to the **C** band, and can be described by a smooth transition from $S_1(^1A'')$ to $S_3(2\,^1A')$ excitation (Fig. 5). (v) When comparing the vector properties and rotational distributions of NO following excitation in the **B** and **D** bands (see Table I, Figs. 6, 8, and 9, and Ref. 11), we can make several predictions which are all borne out by experiments: (a) when monitoring NO[($v''=0$, $Q_{11}(33.5)$], the S_1 component is smaller relative to S_3 than when monitoring $Q_{22}(33.5)$ in accord with the observation that $[\mathrm{NO}(\Pi_{1/2})] < [\mathrm{NO}(\Pi_{3/2})]$ with **D** band excitation; (b) the parallel component increases with decreasing wavelength for $v''=0$; (c) R_{11} and R_{22} show less S_3 character than Q_{11} and Q_{22}, as expected from the Λ-doublet propensities.

Thus, all the experimental evidence supports the assignments of both the **D** and **C** bands to excitations to $S_1(^1A'')$. We also note that although the S_1 state is dissociative, it has a shallow minimum and thus resembles the S_1 state of the alkyl nitrites. The latter is also dissociative on a subpicosecond time scale, but nevertheless gives rise to a vibrational progression.[22]

In conclusion, we find that all the observed transitions involve excitations from orbitals centered on the Cl atom to NO π^* orbitals. The degree of Cl→NO charge transfer in the excited state varies from case to case (Table IV), being the largest for **B** band excitation. We note, however, that excitations involving promotion of an electron from MO 15 to MO 17 or 18 have small oscillator strengths. The reason for the low transition probability is most likely the poor overlap between the relevant electronic wave functions; MO 15 has most of its electron density around Cl, in the NOCl plane perpendicular to the N–Cl bond. MO 17 (NO π_z^*) on the other hand, has most of its charge density perpendicular to the ClNO plane, and the overlap is not as good as for the stronger transitions as can be visualized with the aid of Fig. 10.

B. Implications to photodissociation dynamics

Since the dynamics of photofragmentation depends on the nature of the PES along the reaction coordinate, some comments on the influence of the electronic structure of NOCl on its photodissociation dynamics are in order. The values of the β parameters suggest that dissociation on all the surfaces is fast compared with the parent rotational period, and thus the dynamics is dominated by the forces and motions of the photofragments on the excited PES.

The spin–orbit population ratios $[\mathrm{NO}(^2\Pi_{1/2})]/[\mathrm{NO}(^2\Pi_{3/2})]$ exhibit propensities that depend strongly on the nature of the excited electronic state. NO($^2\Pi_{3/2}$) is predominantly populated in dissociation on $T_1(1\,^3A'')$, and its population is also significantly greater than that of NO($^2\Pi_{1/2}$) in dissociation on $S_1(1\,^1A'')$ (**D** and **C** band excitations). With excitation in the **B** band [$S_3(2\,^1A')$ excited state], however, the two spin–orbit states have rather similar populations with a slight preference for NO($^2\Pi_{1/2}$). These propensities cannot be explained trivially by state correlations (Hund's case c),[10] and more likely reflect also the couplings and uncouplings of surfaces along the reaction coordinate. A correlation between the NO($^2\Pi_{1/2,3/2}$) and Cl($^2P_{1/2,3/2}$) states should be most revealing, and Bruno *et al.* got a better fit for the **D** band Doppler profiles by assuming that only Cl($^2P_{3/2}$) is produced.[10(a)] Unfortunately, the resolution in our present sub-Doppler experiments is insufficient to deconvolute the contributions of the two spin–orbit states of Cl which are separated by 880 cm^{-1}. With TOF-MPI detection, better energy resolution can be achieved, and such experiments will be carried out in the future.

Fragments' V,R energy distributions also depend intimately on the nature of the excited PES. The NO($v''=0$) rotational distributions obtained with excitation in the **D** (500 nm) and **B** (355 nm) bands are bell shaped and inverted with maxima at $J''=29.5$ and 43.5, respectively. Such high rotational excitations are a manifestation of a large torque exerted on the NO fragment, and indicate considerable angular anisotropy in the PES along the reaction coordinate.[10,23] A strikingly different behavior is observed in the dissociation on $T_1(1\,^3A'')$ where low J's are mainly populated (Fig. 7). This behavior is typical of dissociation on a PES without large angular anisotropy,[23,24] implying that the force is exerted near the NO center of mass. The different rotational distributions obtained in dissociation on $T_1(1\,^3A'')$ and $S_1(1\,^1A'')$ are all the more noteworthy, since both states derive from the same electronic configuration.

Dissociation on T_1 is particularly intriguing since it exhibits state-specific behavior with regard to the initially excited bending and stretching vibrations on T_1.[14] The *rotational* distributions are multimodal and depend only on the number of *bending* quanta, while NO *vibrational* excitation depends only on the number of *stretching* quanta in the excited parent. Vibrational adiabaticity appears also in dissociation on $S_1(1\,^1A'')$; NO($v''=1$) is apparently correlated with excitation of NO stretch in the parent S_1 state, and gives rise to the **C** absorption band. The product state distributions will be examined in detail both experimentally and theoretically, with special attention to the role of surface crossings between T_1 or S_1 and the linear $T_2(1\,^3A')$ surface (Table

II and Fig. 11). Another intriguing feature revealed in the geometry optimized calculations is the existence of shallow minima along the reaction coordinate on the T_1 and S_1 surfaces. The experimental results, nevertheless, indicate that dissociation is fast. The motions on the dissociative surfaces and possible crossings with T_2 are being examined theoretically for these two surfaces. A full description of the photodissociation dynamics on T_1, S_1 and S_2 will be reported separately.

The Λ-doublet population ratios can provide insights into the orientations of the singly occupied MOs in the excited parent, and possible electron reorganization during the dissociation. We find that in almost all cases, the Λ-doublet propensities can be rationalized based on the initially excited MOs. Thus, despite the existence of strong couplings between fragment translation and rotation (final state interactions) that result in high rotational excitation in the **B** and **D** states, the initial orientation of the excited NO π^* lobe in NOCl is preserved in the NO products. A notable exception is the absence of Λ-doublet preference in NO ($^2\Pi_{3/2}$) produced via excitation in the **D** band [i.e., on the $S_1(1\,^1A'')$ surface]. As discussed above, the loss of orientation may derive from state-specific perturbations, possibly by $T_2(1\,^3A')$ which crosses the $S_1(1\,^1A'')$ surface at large Cl–N separations (Fig. 11).

V. CONCLUSIONS

The following assignments are proposed for the electronic spectrum of NOCl in the 620–180 nm wavelength region:

(1) $T_1(1\,^3A'') \leftarrow S_0(1\,^1A')$:(**E** band); $\nu_1' = 1580\ \text{cm}^{-1}$, $\nu_3' = 380\ \text{cm}^{-1}$. A series of weak bands with diffuse structure at ~612–560 nm. The transition borrows intensity by mixing with remote singlet states, predominantly the $4\,^1A'$ state.

(2) $S_1(1\,^1A'') \leftarrow S_0(1\,^1A')$ (**D** and **C** bands); two peaks at 470 and 440 nm, corresponding to $\nu_1' = 1670\ \text{cm}^{-1}$.

(3) $S_3(2\,^1A') \leftarrow S_0(1\,^1A')$ (**B** band); a strong broad band with no discernible structure, and a peak at ~340 nm.

(4) $S_5(4\,^1A') \leftarrow S_0(1\,^1A')$ (**A** band); a very strong, broad band with no structure that peaks at ~200 nm.

The *ab initio* CI calculations indicate that the T_1 and S_1 surfaces have shallow minima, while the other surfaces are purely repulsive. The measurements of the vector properties suggest that dissociation on the T_1, S_1, and S_3 surfaces is much faster than a rotational period, and theoretical and experimental studies of the photodissociation dynamics are now being pursued.

ACKNOWLEDGMENTS

The authors wish to thank R. W. Field and H. Lefebvre-Brion for discussions regarding intensity borrowing.

[1] P. L. Houston, J. Phys. Chem. **91**, 5388 (1987), and references cited therein.
[2] J. P. Simons, J. Phys. Chem. **91**, 5378 (1987).
[3] (a) R. N. Zare and D. R. Herschbach, Proc. IEEE **51**, 173 (1963); (b) R. N. Zare, Mol. Photochem. **4**, 1 (1972).
[4] C. H. Greene and R. N. Zare, Ann. Rev. Phys. Chem. **33**, 119 (1982).
[5] R. N. Dixon, J. Chem. Phys. **85**, 1866 (1986).
[6] (a) P. Andresen and E. W. Rothe, J. Chem. Phys. **82**, 3634 (1985); (b) M. H. Alexander and P. J. Dagdigian, *ibid.* **80**, 4863 (1984); (c) M. H. Alexander *et al.*, *ibid.* **89**, 1749 (1988).
[7] C. F. Goodeve and S. Katz, Proc. R. Soc. London Ser. A **172**, 432 (1939).
[8] D. Solgadi, F. Lahmani, C. Lardeux, and J. P. Flament, Chem. Phys. **79**, 225 (1983).
[9] G. E. Busch and K. R. Wilson, J. Chem. Phys. **56**, 3655 (1972).
[10] (a) A. E. Bruno, U.Bruhlmann, and J. R. Huber, Chem. Phys. **122**, 155 (1988); (b) A. Ticktin, A. E. Bruno, U. Bruhlmann, and J. R. Huber, Chem. Phys. **125**, 403 (1988).
[11] A. Ogai, C. X. W. Qian, L. Iwata, and H. Reisler, Chem. Phys. Lett. **146**, 367 (1988).
[12] C. X. W. Qian, A. Ogai, H. Reisler, and C. Wittig, J. Chem. Phys. **90**, 1 (1989).
[13] G. Herzberg, *Spectra of Diatomic Molecules* (Van Nostrand, New York, 1950).
[14] C. X. W. Qian, A. Ogai, L. Iwata, and H. Reisler, J. Chem. Phys. **89**, 10 (1988).
[15] T. H. Dunning, Jr., J. Chem. Phys. **53**, 2823 (1970).
[16] J. S. Binkley, R. A. Whiteside, R. Krishnan, R. Seegar, D. J. Defrees, H. B. Schlegel, S. Topiol, L. R. Kahn, and J. A. Pople, Gaussian Inc., Carnegie Mellon University, Pittsburgh, PA (1982).
[17] J. J. Diamond, G. A. Segal, and R. W. Wetmore, J. Phys. Chem. **88**, 3532 (1984).
[18] (a) V. Marudarajan and G. A. Segal, Chem. Phys. Lett. **128**, 1 (1986); (b) S. Nagamani and G. A. Segal, J. Am. Chem. Soc. **108**, 6880 (1986).
[19] D. J. Millen and J. Pannell, J. Chem. Soc. 1322 (1961).
[20] N. M. Ballash and D. A. Armstrong, Spectrochim. Acta Part A **30**, 941 (1974).
[21] H. Lefebvre-Brion and R. W. Field, *Perturbations in the Spectra of Diatomic Molecules* (Academic, New York, 1986), Chap. 5.
[22] H. Reisler, M. Noble, and C. Wittig, in *Molecular Photodissociation Dynamics* (Royal Society of Chemistry, London, 1987), p. 137 and references cited therein.
[23] (a) R. Schinke, Annu. Rev. Phys. Chem. **39**, 39 (1989), and references cited therein; (b) R. Schinke and V. Engel, Faraday Discuss. Chem. Soc. **82**, 111 (1986).
[24] P. Andresen and R. Schinke, in Ref. 22, p. 61.